The Design and Optimization of Optical Filters for High Data Rates Optical Systems

The Design and Optimization of Optical Filters for High Data Rates Optical Systems

Edited by

Fethallah Karim

Cambridge Scholars Publishing

The Design and Optimization of Optical Filters for High Data Rates Optical Systems

Edited by Fethallah Karim

This book first published 2019

Cambridge Scholars Publishing

Lady Stephenson Library, Newcastle upon Tyne, NE6 2PA, UK

British Library Cataloguing in Publication Data
A catalogue record for this book is available from the British Library

ISBN (10): 1-5275-2210-5
ISBN (13): 978-1-5275-2210-7

TABLE OF CONTENTS

A SYNTHESIS OF DISPERSION-COMPENSATING TRIANGULAR LATTICE INDEX-GUIDING PHOTONIC CRYSTAL FIBERS USING THE DIRECTED TABU SEARCH METHOD

FETHALLAH KARIM[1]
LABORATORY OF TELECOMMUNICATIONS, FACULTY OF TECHNOLOGY, ABOUBEKR BELKAID UNIVERSITY, CHETOUANE, TLEMCEN, ALGERIA

Abstract

In this paper, triangular lattice index-guiding photonic crystal fibers (PCFs) are synthesized to compensate the chromatic dispersion of a single mode fiber (SMF-28) for an 80km optical link operating at 1.55 µm, by using the directed Tabu Search algorithm. Hole-to-hole distance, circular air-hole diameter, solid-core diameter, ring number, and PCF length parameters are optimized for this purpose. Three synthesized PCFs with different physical parameters are compared in terms of their objective function values, residual dispersions, compensation ratios, and confinement losses.

Keywords: *Triangular lattice index-guiding photonic crystal fiber; dispersion compensation; directed Tabu Search; synthesis.*

1. Introduction

The chromatic dispersion of optical fibers is one of the most important parameters for optical communication systems because of its strong influence on high data rate transmission systems. To remedy this problem, specific optical fibers with various dispersion profiles have been proposed for dispersion compensation and optical switching applications: such as

[1] Email: karim.fethallah@gmail.com

chirped Fiber Bragg Gratings (FBGs) [1–4], dispersion compensating fibers (DCFs) [5, 6], photonic crystal fibers (PCFs) [7–9], and so on.

Photonic crystal fibers (PCFs) [10, 11] that consist of a central defect region surrounded by multiple air holes that run along the fiber length have attracted much attention in recent years because of their unique properties, which have not been realized in conventional optical fibers. PCFs are divided into two different kinds of fibers. The first one, index-guiding PCF, guide light using a total internal reflection between a solid core and a cladding region with multiple air-holes [12, 13]. The second one uses a perfect periodic structure that exhibits a photonic band-gap (PBG) effect at its operating wavelength in order to guide light in a low index core-region [14, 15].

The aim of this work is to synthesize index-guiding PCFs with triangular lattices that have been formed by circular air-holes through the use of the Directed Tabu Search (DTS) method. A comparison between the synthesized PCFs performances will be made in order to find the best synthesized dispersion-compensating PCF. Our goal is to minimize the chromatic dispersion of an 80km optical link by placing the synthesized dispersion-compensating PCFs after a single mode fiber (SMF-28) operating at 1.55 μm. For wavelength division multiplexing (WDM) applications, PCFs should provide high negative dispersion values and a negative dispersion slope over a large wavelength range. Our optimization problem consists in the minimization of the residual dispersion over a wavelength range of 100nm (1.5μm–1.6 μm).

In this work, the directed Tabu Search (DTS) has been applied for the first time in the synthesis and optimization of PCFs physical parameters for dispersion compensation applications. More details about this hybrid method will be presented in section 2 of this article. We note that a genetic algorithm, combined with a full-vectorial finite-element solver, to design PCFs for broadband dispersion compensation in a generic stretcher–compressor system of an ytterbium fiber laser has already been presented in reference 16.

2. Synthesis of triangular lattice index-guiding PCFs using the Directed Tabu Search

This section deals with the synthesis of physical parameters in index-guiding PCFs characterized by triangular lattices and circular air holes. This kind of PCF is reconstructed with a negative chromatic dispersion that should reduce the positive chromatic dispersion occurring from a single mode fiber. Let us take the example of a standard SMF-28™ that provides a positive dispersion of 1390.2 ps/nm.km at the 1.55 µm wavelength for an 80 km optical link. This fiber has a positive dispersion slope S_0 of 0.092 ps/ nm^2.km and a zero-dispersion value of λ_0= 1.3115 µm. The SMF-28™ dispersion approximately equals [17]

$$D_{SMF}(\lambda) \approx \frac{S_0}{4}\left[\lambda - \frac{\lambda_0^4}{\lambda}\right] \tag{1}$$

Our optimization problem then consists of the minimization of the residual dispersion over a wavelength range that extends from λ=1.5 µm to λ=1.6 µm. The objective function (residual dispersion) can be written as

$$\text{Objective function} = D_{SMF}(\lambda)\times L_{SMF} + D_{PCF}(\lambda)\times L_{PCF} \tag{2}$$

where L_{SMF} equals 80km.

To reconstruct a PCF with a negative dispersion value and a negative dispersion slope, the directed Tabu Search (DTS) is applied to synthesize four physical parameters of this device: hole-to-hole distance, Λ (or pitch); air-hole diameter, d (or air-filling fraction, d/Λ); solid-core diameter, d_{co}; and ring number, N_r. We note that the synthesized negative dispersion is obtained for a 1km PCF length. The SMF-28 positive dispersion value is perfectly compensated at the 1.55µm wavelength by adjusting the PCF length L_{PCF}, according to the synthesized negative dispersion value and a zero-residual dispersion at the operating wavelength.

The Directed Tabu Search (DTS) method has been chosen for synthesis according to their good performances, as previously demonstrated in references 18 and 19. This method has been described for the first time in reference 20. It has been applied to estimate the thermo-optic coefficient and thermal expansion coefficient of a chirped Fiber Bragg Grating [19]; the hybrid Tabu Search algorithm has also been used to optimize the strain profiles of a sampled Bragg grating [19]. The performances generated from this method have been compared with those of other hybrid metaheuristics in references 18 and 19. DTS has given the best objective function with a minimum evaluation function number. This comparison has proved that DTS is advantageous in higher dimensional systems.

DTS is a memory-based hybrid algorithm, it uses the Adaptive Pattern Search (APS) based on the Approximate Descent Direction (ADD) and the Nelder-Mead (NM) search in its exploration of neighborhood-local search strategies in order to generate trial points. The Nelder-Mead algorithm is used in the DTS intensification as a local search strategy to refine the best solutions visited so far. A Tabu List (TL) is introduced to save and rank solutions due to their immediacy and their objective function values. Therefore, some positions in the TL are kept for visited solutions, which helps the intensification scheme to refine the search from these solutions at the final stage. Within each solution saved in the TL, two types of regions are specified in the search space. The first one is a Tabu Region (TR) in which no new trial point is allowed to be generated. The other is a Semi-Tabu Region (Semi-TR) that comprises of the region around the TR. The main role of Semi-TRs is to generate neighboring trial points in a special way so that returning to a visited TR is avoided when the trial solution lies inside a Semi-TR.

Figure 1 illustrates the cross-section of three synthesized triangular lattice solid-core PCFs: showing the core and cladding permittivity, ε, and distribution. We have chosen only three PCFs, which are the best optimized following several simulation trials using the DTS. These PCFs will be compared according to their synthesized physical parameters, objective function values, residual dispersions, compensation ratios, PCF-to-SMF length percentages, and confinement losses. We note that the air-holes are periodically distributed along the x and y axes and homogeneously distributed along the z-axis. We have only considered the Transverse Magnetic (TM) propagation mode; therefore, the electric field E_z propagates according to the z-axis direction, while the magnetic fields, H_x and H_y, propogate along the x-axis and y-axis directions, respectively. We remark from fig. 1 that the pitch, air-hole diameter, solid-core diameter and, consequently, the air-holes number are different for each synthesized PCF. In our work, the Finite Difference Time Domain (FDTD) method is used for the analysis of the PCFs. This method is an approach that directly solves Maxwell's equations through the proper discretization of both time and space domains [21]. Since PCFs are considered to be two-dimensional photonic crystals, the PCF cross-section is divided into several grid cells along the x and y axes. The grid cell number is taken to 400 along each axis (see fig. 1), while the total number of time steps equals 4000.

It has been already demonstrated that triangular PCFs are an endlessly single mode, where only the fundamental mode is guided for any wavelength, if their air-filling fraction, d/Λ, is lower than 0.406 [22– 23].

However, since all synthesized air-filling fractions are higher than this value, it is evident that these PCFs present higher-order modes.

The normalized frequency V is another parameter that determines whether a PCF presents a single fundamental mode or other higher-order modes. This parameter can be written as follows [24]

$$V = \frac{2\pi}{\lambda}\Lambda\sqrt{n^2_{eff} - n^2_{FSM}} \quad (3)$$

where Λ, n_{eff}, n_{FSM} are the pitch, the effective index of the fundamental guided mode, and the effective index of the fundamental space-filling mode (FSM), respectively.

A PCF is a single mode if V < 2.405 [17] and it becomes a multimode if V> 2.405. It has been shown that in triangular PCFs the second-order mode effective transverse wavelength, which is related to the dimension of the defect region , is $\lambda^* \approx 2\Lambda$ at the cutoff condition. As a consequence, the normalized cutoff frequency becomes $V^* = \frac{2\pi}{\lambda^*}\Lambda \approx \pi$ [17]. According to the synthesized PCFs apparition order in fig. 1, the cutoff condition of the second-order mode of the three synthesized PCFs is $\lambda_1^* = 1.02$ µm, $\lambda_2^* = 0.78$ µm and $\lambda_3^* = 0.88$ µm, respectively.

Table 1 indicates the numerical simulation results that concern the three synthesized dispersion-compensating PCFs already presented in fig.1. We note that the apparition order in fig.1 is respected in table 1. We note also that the initial search intervals of the PCF parameters, which have been used in the DTS optimization are as follows: 0.6<Λ(pitch)<0.9 µm, 0<d/Λ (air-hole diameter to pitch ratio)< 0.6, 1<N_r(ring number)<10, and 0<d_{core} (core diameter)< 1 µm.

It has been demonstrated in reference 17 that when the pitch value, Λ, is lower than 1µm, the chromatic dispersion value of triangular PCFs is always negative from 1200nm to 1600nm. The authors have used this equation (6) to represent the chromatic dispersion (CD) over the operating wavelength range, where the effective refractive index n_{eff} (which depends on the pitch, the hole diameter, the solid core diameter, and the number of rings) was computed through a software code based on the FDTD method over the same wavelength interval. Since the synthesized hole-to-hole distance values are all lower than 1µm, the three PCFs present negative dispersion values over the wavelength range 1.5µm–1.6µm. It is important to remember that the aim of this study is to minimize the residual dispersion value over this wavelength range. Since the optical signal attenuation is lowest on the 1.55µm wavelength we are interested in presenting the optimized PCFs numerical simulation results at this operating wavelength. In order to fulfil this, we have used a SMF of 80km operating at 1.55µm (third window).

We have indicated that from table 1 the DTS has given the lowest objective function value for PCF1, if we place PCF1 after the SMF we still have a residual dispersion of -5.27ps/nm at 1.55µm. PCF3 has given the best residual dispersion (-1.43ps/nm) at the operating wavelength. We have noted that the PCF dispersion is synthesized for a 1km PCF length. The residual dispersion is perfectly minimized at 1.55µm, when the exact PCF length is determined from the residual dispersion relationship as follows:

$$L_{PCF} = D_{SMF}(1.55) \times L_{SMF} / D_{PCF}(1.55) \quad (4)$$

where L_{SMF}=80 km and D_{SMF} (1.55) =1390.2ps/nm.

By using the equation from reference 4, we have found that the corresponding PCF1, PCF2, and PCF3 lengths are 0.9962km, 1.0024km, and 0.9989km, respectively, which gives a PCF-to-SMF length percentage of 1.245%, 1.253%, and 1.248%, respectively.

In WDM applications, the positive dispersion and the positive dispersion slope of a SMF should be compensated at the same time by a PCF negative dispersion and a PCF negative dispersion slope. A PCF dispersion slope is considered negative when the slope stays inversely proportional along the whole wavelength range. A triangular PCF presents a positive dispersion slope when its slope curve remains positive when it starts from a particular wavelength. Therefore, this PCF cannot be used in WDM dispersion compensation due to the fact that it cannot give the available negative dispersion at each WDM wavelength. To verify this aspect, the compensation ratio (CR) will be calculated. This parameter should be near to 1 over the operating wavelength interval, which means that the negative dispersion at each wavelength has been correctly compensated. CR(λ) is the fraction of the SMF dispersion which the PCF compensates at wavelength λ, that is [17]

$$CR(\lambda) = \frac{D_{SMF}(\lambda)}{D_{SMF}} \times \frac{D_{PCF}}{D_{PCF}(\lambda)} \tag{5}$$

Figure 2 illustrates the CR plot of the three synthesized PCFs. We can note from this figure that the best compensation ratio is obtained for all reconstructed PCFs at the operating wavelength (CR (1.55) =1). Since PCF1 presents the highest residual dispersion average and maximum error, we remark from fig. 2 that PCF1 presents the highest CR values when it is compared with PCF2 and PCF3. PCF2 presents the minimum residual dispersion average error over the operating wavelength range.

Figure 3 illustrates the dispersion curves of the three synthesized triangular lattice solid-core PCFs. Here, the chromatic dispersion (CD) is calculated from the real part of the complex effective index, n_{eff}, as [25]

$$CD(\lambda) = -\frac{\lambda}{c} \times \frac{d^2 \operatorname{Re}(n_{eff})}{d\lambda^2} \tag{6}$$

where c is the velocity of light in a vacuum.

We remark from fig. 3 that PCF1, PCF2, and PCF3 present negative dispersion values and negative dispersion slopes over the wavelength range 1.5µm–1.6µm. We can, therefore, conclude that the three synthesized PCFs are suitable for dispersion compensation in WDM transmission systems.

In solid-core PCFs, light is confined within a core region by the air-holes. Light will move away from the core if the confinement provided by the air-holes is inadequate. This means that it is important to design the air-hole diameter and hole-to-hole spacing aspects of the PCF structure in order to realize low-loss PCFs. In particular, the ratio between the air-hole diameter and the pitch must be designed to be large enough to confine light in its core [17]. Figure 4 presents the confinement loss curves of the three synthesized PCFs. The confinement loss (CL) is calculated from the imaginary part of the complex effective index, n_{eff}, as [25]

$$CL(\lambda) = 8.686 \times \operatorname{Im}(k_0 n_{eff}) \tag{7}$$

where k_0 is the free space wave number.

It has been demonstrated in reference 17 that the CL quickly decreases when the air-hole ring number (N_r) or the air-hole diameter (d) increases. The reduction rate of the confinement loss increases in the same way with these geometric parameters. As demonstrated in fig. 4, the PCF2 confinement loss values are a little higher than the other PCFs confinement losses over the operating wavelength range because of the PCF2 synthesized pitch (Λ) and the small core diameter (d_{co}) values. PCF3 is characterized by the smallest CL values when it is compared with PCF1 because the PCF3 synthesized ring number (N_r=7) is higher than PCF1 (N_r=6). In this case, we have noted that the ring number impact on the CL reduction rate is much higher than on the other parameters.

We can remark from fig. 4 that all three synthesized PCFs present acceptable confinement loss values (about an average value of 1.5dB/Km) starting from a wavelength of 1.54µm. We have noted that the confinement loss is close to 0dB for the three PCFs from 1.5µm to 1.54µm. When the imaginary part of the effective index was computed through the FDTD algorithm over the operating interval 1.5–1.6µm, the refractive index underwent a significant increase (starting from 1.54µm), which consequently affected the confinement loss parameter; this is in addition to the fact that the relationship between the two parameters is linear (see equation 7). The confinement loss can be enhanced by increasing the solid core diameter. The appearance of the CL average value (between 1.54µm and 1.6µm) is justified by the small core diameters (less than 1 µm) which characterize the three PCFs. When a PCF core diameter becomes too small, the silica region inside the first ring, in spite of the large surrounding air-holes, is unable to confine the field and this forces an amount of light to propagate outside the solid core.

Table 1. Numerical simulation results of the three synthesized dispersion-compensating PCFs

	Λ= 0.51 μm; d/Λ= 0.5688; d_{co}= 0.73 μm; N_r= 6 PCF1	Λ= 0.39 μm; d/Λ= 0.5641; d_{co}= 0.56μm; N_r= 8 PCF2	Λ= 0.44 μm; d/Λ= 0.5662; d_{co}= 0.63 μm; N_r= 7 PCF3
Objective function value	4.07×10^2	5.90×10^2	6.11×10^2
Residual dispersion at 1.55μm for 1km PCF length (ps/nm)	-5.27	3.37	-1.43
Optimized PCF length at 1.55μm (km)	0.9962	1.0024	0.9989
PCF-to-SMF length percentage at 1.55μm (%)	1.245	1.253	1.248
Residual dispersion average and maximum error	-1.83/8.83	-1.01/7.25	-3.47/7.18

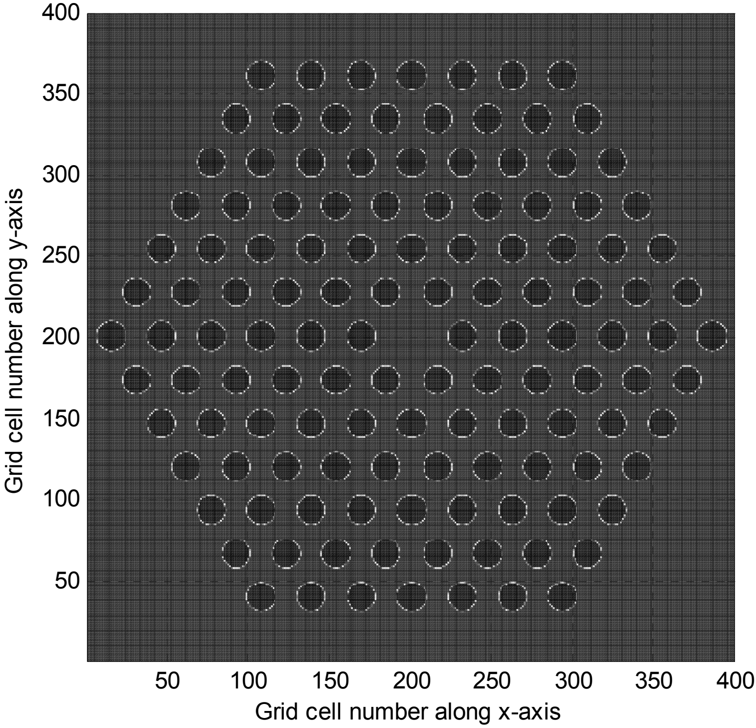

(a) Λ= 0.51 μm; d/Λ= 0.56; d_{co}= 0.73μm; N_r= 6

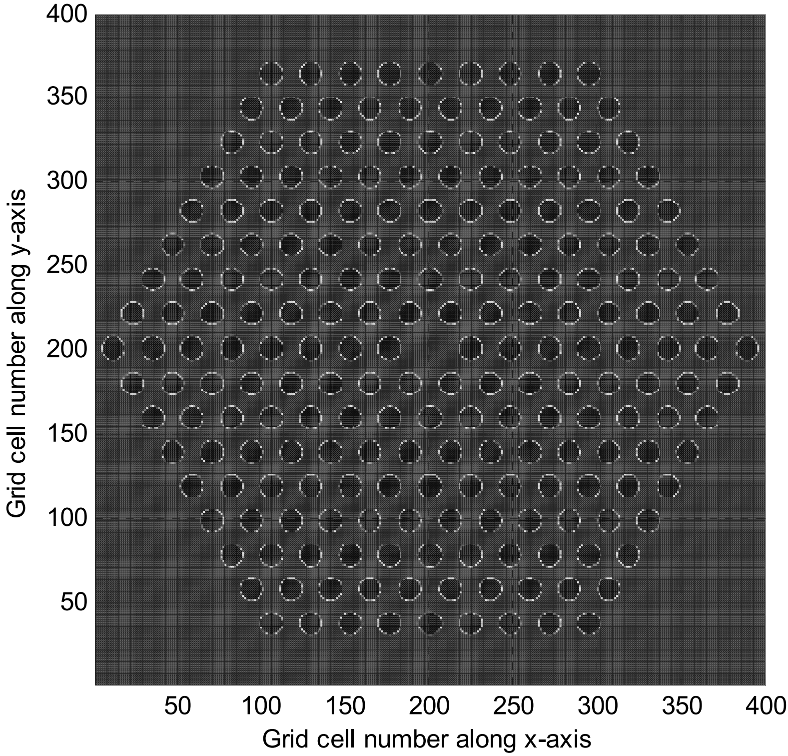

(b) Λ= 0.39µm; d/Λ= 0.56; d_{co}= 0.56µm; N_r= 8

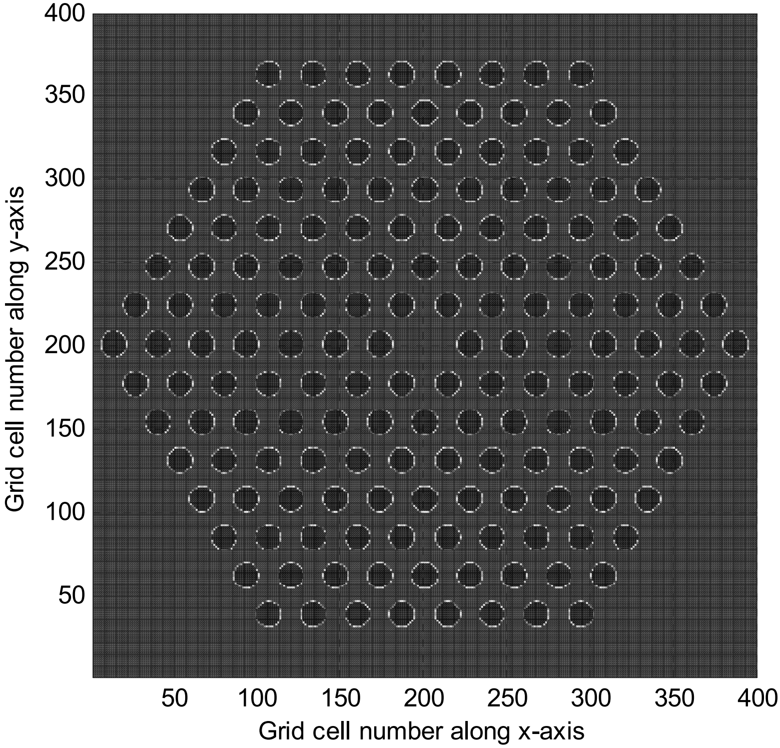

(c) Λ= 0.44µm; d/Λ= 0.56; d_{co}= 0.63µm; N_r= 7

Fig. 1: Core and cladding permittivity distribution of the three synthesized triangular lattice solid-core PCFs

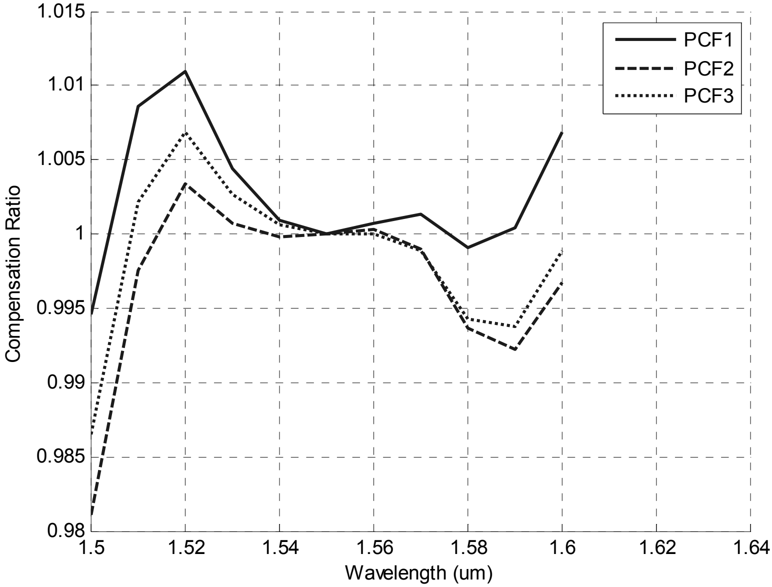

Fig. 2: The compensation ratio of the three synthesized triangular lattice solid-core PCFs

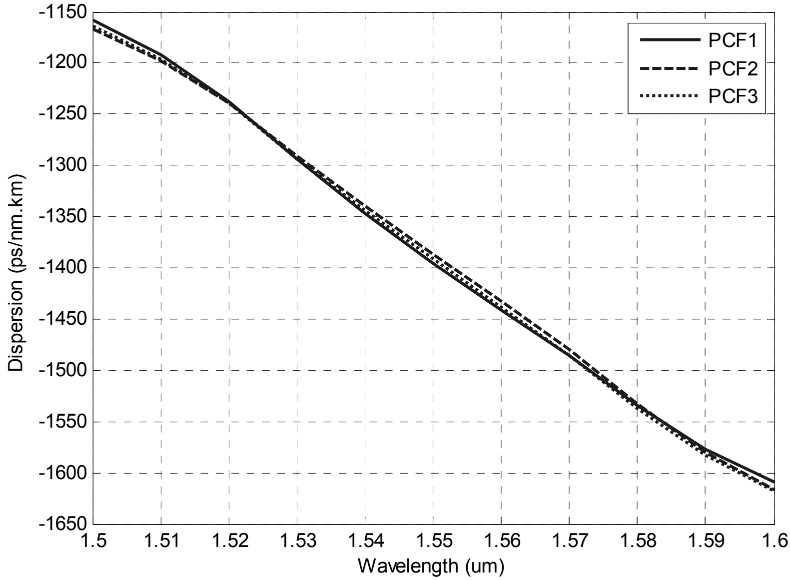

Fig. 3: The dispersion of the three synthesized triangular lattice solid-core PCFs

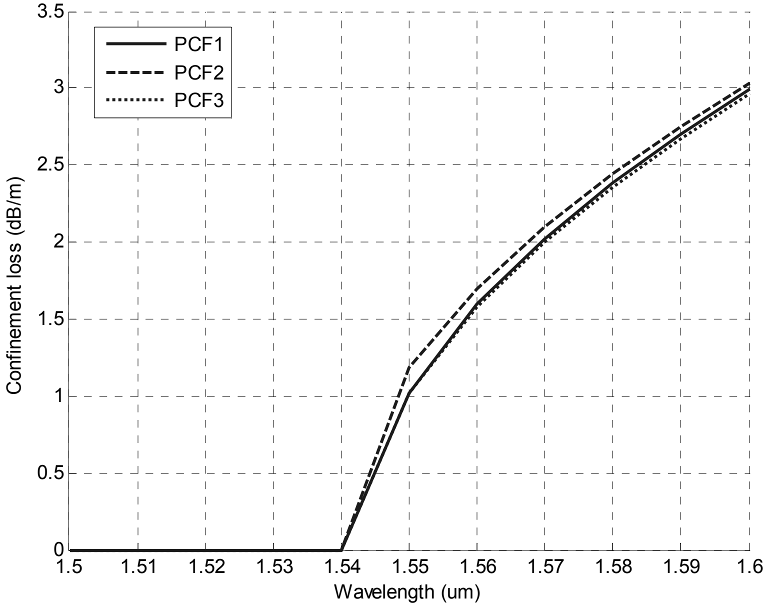

Fig. 4: The confinement loss of the three synthesized triangular lattice solid-core PCFs

3. Conclusion

In this paper, three synthesized dispersion-compensating triangular lattice index-guiding PCFs have been compared according to their objective function values, residual dispersions, compensation ratios, and confinement losses. The Directed Tabu Search (DTS) has been used to synthesize the pitch, the circular air-hole diameter, the solid-core diameter, and the ring number. We have noted that all synthesized PCFs do not conform to an endlessly single mode, as they present other higher-order modes according to their cut-off conditions. We note that a PCF-to-SMF length percentage of only 1.25% has been obtained in order to compensate the chromatic dispersion of the 80km optical transmission link. In a single mode transmission system that is centered on 1.55µm, PCF3 is considered as the best dispersion compensating fiber with a residual dispersion of -1.43ps/nm.km. Despite it was reconstructed with the highest objective function value, while PCF2 is the best dispersion compensating fiber in a

WDM transmission system because it presents the minimum residual dispersion average error over the whole operating wavelength range of 1.5µm–1.6µm. We have mentioned that the three synthesized PCFs present the best compensation ratio (CR=1) at a 1.55µm wavelength. We have also noted that all synthesized PCFs present an average confinement loss value of 1.5dB/m over the operating wavelength range. Since all synthesized core diameter values are lower than 1µm, we consider the confinement loss average value to be too high. The confinement loss can be reduced by increasing the PCF core diameter or the ring number.

References

[1] M. Sumetsky and B.J. Eggleton, "Fiber Bragg Gratings for dispersion compensation in optical communication systems,'' Journal of Optical and Fiber Communications Research.**2**, 256-278, (2005).

[2] Z. Zang, "All-optical switching in Sagnac loop mirror containing an ytterbium-doped fiber and Fiber Bragg Grating," Applied Optics. **52**, 5701-5706, (2013).

[3] Z. Zang and Y. Zhang, "Analysis of optical switching in a Yb^{3+} doped Fiber Bragg Grating by using self-phase modulation and cross-phase modulation," Applied Optics. **51**, 3424-3430, (2012).

[4] Z. Zang and Y. Zhang, "Low-switching power (<45 mW) optical bistability based on optical nonlinearity of ytterbium-doped fiber with a fiber Bragg grating pair," Journal Of Modern Optics.**59**,161-165,(2012).

[5] L. Grüner-Nielsen et al, "Dispersion-Compensating Fibers," Journal of Lightwave Technology.**23**,3566, (2005).

[6] P. Palai, "A Dispersion Flattening Dispersion Compensating Fiber Design for Broadband Dispersion Compensation," Fiber and Integrated Optics, 20, 21-27, (2001).

[7] Y. Ni et al, "Dual-core photonic Crystal fiber for dispersion compensation," IEEE Photonics Technology Letters. **16**, 1516-1518, (2004).

[8] Y. Liu et al, "A novel multi-waveband dispersion compensating fiber based on hybrid photonic crystal fiber," Optoelectronics Letters.**9**, 53-56, (2013).

[9] M. Mejbaul Haque et al, "Design and characterization of single mode circular photonic crystal fiber for broadband dispersion compensation**,"** Optik - International Journal for Light and Electron Optics. 125,2608-2611, (2014).

[10] J. Broeng, D. Mogilevstev, S.E. Barkou, and A. Bjarklev, “Photonic crystal fibers: A new class of optical waveguides,” Optical Fiber Technology. **5**, 305-330, (1999).

[11] T.A. Birks, J.C. Knight, B.J. Mangan, and P.St.J. Russell, “Photonic crystal fibers: An endless variety,” IEICE Trans. Electron. **E84-C**, 585-592, (2001).

[12] J.C. Knight, T.A. Birks, P.St.J. Russell, and D.M. Atkin, “All-silica single-mode optical fiber with photonic crystal cladding,” Optics Letters. **21**, 1547-1549, (1996).

[13] T.A. Birks, J.C. Knight, and P.St.J. Russell, “Endlessly single-mode photonic crystal fiber,” Opt. Lett. **22**, 961-963, (1997).

[14] J.C. Knight, J. Broeng, T.A. Birks, and P.St.J. Russell, “Photonic band gap guidance in optical fiber,” Science **282**, 1476-1478, (1998).

[15] R.F. Cregan, B.J. Mangan, J.C. Knight, T.A. Birks, P.St.J. Russell, P.J. Roberts, and D.C. Allan, “Single mode photonic band gap guidance of light in air,” Science. **285**, 1537-1539, (1999).

[16] R.R. Musin, A.M. Zheltikov, “Designing dispersion-compensating photonic-crystal fibers using a genetic algorithm,” Optics Communications. **281**, 567–572, (2008).

[17] F. Poli, A. Cucinotta, and S. Selleri, “Photonic Crystal Fibers: Properties and Applications,” Springer, The Netherlands, 2007.

[18] F. Karim and O. Seddiki, “Synthesis of chirped apodized Fiber Bragg Grating parameters using Direct Tabu Search algorithm: Application to the determination of thermo-optic and thermal expansion coefficients,” Optics Communications .**283**, 2109-2116, (2010).

[19] F. Karim and O. Seddiki, “Direct Tabu Search algorithm for the Fiber Bragg Grating distributed strain sensing,” Journal of Optics **12**, 095401 (2010).

[20] A. Hedar, M. Fukushima, “Tabu Search directed by direct search methods for nonlinear global optimization,” European journal of Operational Research **170**, 329–349 (2006).

[21] K. Okamoto, “Fundamentals Of Optical Waveguides,” Academic Press, Elsevier, USA, 2006.

[22] B. T. Kuhlmey, R. C. McPhedran, C. M. de Sterke, P. A. Robinson, G. Renversez, and D. Maystre, “Microstructured optical fibers: where’s the edge?,” Optics Express, vol. 10, pp. 1285–1290, 2002.

[23] N. A. Mortensen, J. R. Folkenberg, M. D. Nielsen, and K. P. Hansen, “Modal cutoff and the V parameter in photonic crystal fibers,” Optics Letters, vol. 28, pp. 1879–1881, 2003.

[24] M.D. Nielsen, J.R. Folkenberg, N.A. Mortensen, and A. Bjarklev, "Bandwidth comparison of photonic crystal fibers and conventional single-mode fibers," Optics Express. vol. 12, pp. 430–435, 2004.

[25] K. Saitoh and M. Koshiba, "Chromatic dispersion control in photonic crystal fibers: application to ultra-flattened dispersion," Optics Express. vol. 11, pp. 843–852, 2003.

A DESIGN FOR A TUNABLE HYBRID SOLC FILTER FOR 40 GBPS DWDM OPTICAL SYSTEMS

HADJ SLIMANE ABDERRAHMANE[1]
AND FETHALLAH KARIM
LABORATORY OF TELECOMMUNICATIONS, FACULTY OF TECHNOLOGY, ABOUBEKR BELKAID UNIVERSITY, CHETOUANE, TLEMCEN, ALGERIA

Abstract

In this paper, will present a method to enhance the performance of a hybrid tunable Solc filter for 40Gbps DWDM systems. By using liquid crystal cells with a variable birefringence, we have achieved wavelength tuning for 33 ITU channels, with a 100 GHz frequency spacing (from 1564.69nm to 1530.32nm) via a 10-stage hybrid Solc filter. This device presents a tuning step of 0.1nm by applying a voltage difference of 0.2V. The optical cancelling technique was used to make the 3dB bandwidth tuning between 0.31nm and 1.4nm. The channel's bandwidth is adjusted for different kinds of 40Gbps modulated channels spectra. The 10-stage hybrid Solc filter theoretically provides an insertion loss of 4.6dB, by using polarizers and birefringent plates that are characterized by high anti-reflection coatings, while its crosstalk approximates 14dB. The proposed filter provides very low polarization dependent loss (PDL) through the incorporation of a polarization beam splitter (PBS) and a polarization beam combiner (PBC).

Keywords: hybrid Solc filter; wavelength tuning; electro-optic effect; bandwidth tuning; insertion loss.

---

[1] Corresponding author email: abderrahmane.hadjslimane@gmail.com

I. Introduction

Several design techniques have previously been used for manufacturing tunable optical filters [1–3]. However, in order to use these filters when switching and add/drop multiplexing devices, they should provide a variable channel bandwidth that matches the different modulation formats that are generated by high data rate optical modulators. At the same time, there needs to be a very high precision used when tuning the appropriate wavelength in order to isolate one channel from several DWDM channels to complete a dropping operation or a switching function. Two arrayed waveguide grating filters that had a variable bandwidth (from 0.05nm to 1nm and from 0.25nm to 60nm) were reported [4–5]. Fiber Bragg Gratings (FBG) are widely used due to their excellent amplitude-filter characteristics. We also noted that the FBG filter was characterized by a variable bandwidth between 0.1nm and 15nm [6–7]. A tunable bandwidth optical filter that was implemented with a micro-electromechanical system (MEMS) was also reported. The bandwidth tuning was achieved with an up-and-down piston motion from the micro mirrors [8]. Another adjustable bandwidth filter was implemented in the planar lightwave circuit (PLC) [9]. A multichannel filter-based Fabry-Perot with a manually variable bandwidth, extending from 1nm to 18nm, and an insertion loss of 3dB has already been commercialized [10]. There is, for example, the Xtract tunable filter manufactured by Anritsu [11], which covers a 1450–1650 nm wavelength range with a wavelength resolution of 0.005nm and can vary a channel's bandwidth from 150 to 650pm [11]. The Xtract filter presents an insertion loss of 6dB and a crosstalk of 40dB [11]. There is also the TFC-C-band narrow tunable filter designed by Teraxion [12], which presents a wavelength tuning accuracy of 0.008nm, a variable 3dB bandwidth between 0.04nm and 0.096nm, an insertion loss of 5dB, and a crosstalk of 25dB [12].

B. Benkelfat et al have experimentally tested the wavelength tunability on C and L bands using a hybrid liquid-crystal Solc filter [13]. R. Hamdi et al proposed an optical cancelling technique in reference 14, which involves the transformation of a half-waved plate to a full-waved one by changing their optical path differences (OPD) providing an electro-optic effect. A ten-stage hybrid Solc filter produced one channel with a full width at half maximum (FWHM) that varies from 2. nm to 11.6 nm, with a wavelength range of 25nm [14]. However, when using a 40Gbps DWDM optical link, the tunable hybrid Solc filter must deliver more narrow bandwidths to transmit and correctly filter the whole signal of the modulated channel. Using the example of three different modulation formats, it has been found that the spectral width should be 0.25nm for a 40Gbps RZ-DPSK channel optical spectrum. This is equal to 0.56nm for a 40Gbps NRZ channel spectrum; however, it should approximate 0.75nm for a 40Gbps RZ-DQPSK modulation [15].

D.F. Bendimerad presented a Tunable-Hybrid-Equalizer Multiple-Passage Birefringent Filter (TMBF) in reference 16. The author proposed a tunable eight stage Lyot filter with four passages (M=4) created by two mirrors placed at the front and the rear sides of the tunable filter. The author used the multiple passages to have a greater number of fixed narrow bandwidths and to enhance the crosstalk of the hybrid lyot filter. The device theoretically offers a minimum FWHM of 0.2 nm and a crosstalk that approximates 5 dB [16]. However, due to the four passages through the eight hybrid stages, the proposed filter suffers from huge insertion and polarization dependent losses.

It is important to remember that the proposed Solc filter in reference 14 presented a bandwidth that varies between 2.6nm and 11.6nm, while the majority of the commercialized tunable filters present a variable bandwidth between 0.25nm and 1nm for 40Gbps optical transmission systems. We also note that this tunable filter presents a wavelength shifting that varies from 1nm to 3nm by applying a voltage difference that varies from 1V to 3V. The wavelength tuning presented in reference 14 is not acceptable in actual reconfigurable high data rates optical networks that need a minimum wavelength tuning step of 0.1nm. The proposed Solc filter in reference 14 does not meet the high data rate conditions that impose very narrow bandwidths and very low wavelength tuning steps. The purpose of our work is to enhance the performance of the hybrid Solc filter presented in reference 14. We have then optimized the geometric parameters of the liquid crystal cell and the calcite plate in the ten hybrid stages in order to achieve a minimal bandwidth of 0.31nm. We have also chosen the available AC voltage values that should be applied by the liquid crystal controller to design a hybrid Solc filter that meets the 100GHz ITU grid standard with a minimal wavelength tuning step of 0.1nm and a variable bandwidth that matches different high data rate modulation formats. The proposed filter will simultaneously produce eight ITU channels on the C-band with an insertion loss lower than 5dB. In the second section of this article, the simulation results of the enhanced filter, with its technical specifications and functionality principle, will be presented and discussed.

II. Functionality of the designed Solc filter

Figure 1 presents a diagram of the tunable filter. The filter's physical configuration is straightforward. In each hybrid stage, a calcite plate is closely placed next to a liquid crystal cell. We must, of course, allow for a small distance between each hybrid stage in order to make a physical distinction between the ten stages. This distance can be fixed (optimized) once the experimentation is complete, according to the insertion loss and the channel's isolation parameters.

For our simulations, in each hybrid stage, we theoretically inserted a fixed birefringent calcite plate with a birefringence δn_{BP} that equals 0.156. We have chosen a geometric thickness e_{BP} of 3.39mm that allows an optical path difference (OPD) of 530µm. The calcite plate used in our simulation is already commercialized by Newlight Photonics [15] and presents an insertion loss of 0.22dB on a C-band. At the same stage, we inserted a nematic liquid crystal cell manufactured by ThorLabs [18]. The E7 nematic cell is driven by a liquid crystal controller. The LC provides a maximal intensity when it is submitted to $25V_{rms}$; however, it provides a maximal retardance when no AC voltage is applied. This cell takes a physical thickness e_{LCC} of 10µm and presents an OPD that varies from 179.8nm to 1210.55nm, when applying an AC voltage of 3.8 V_{rms} and 1.08 V_{rms}, respectively. The liquid crystal also creates an insertion loss of 0.22dB. The ten hybrid stages are alternatively oriented by +/- 45°, according to their horizontal axis, and sandwiched between two crossed linear polarizers. In our simulation, we have chosen two ThorLabs polarizers [18] that are characterized by very high polarization extinction ratios (greater than 30dB) and very low insertion losses (0.087dB).

Figure 2 presents the insertion loss of the eight channels produced by the enhanced Solc filter in a wavelength range of 1530–1565 nm. It is important to note that these channels are initially centered on 1533.08nm, 1537.51nm, 1541.69nm, 1546.29nm, 1550.89nm, 1555.49nm, 1560.09nm, and 1564.69 nm, when w a voltage of 1.08V is simultaneously applied to the ten liquid crystal cells. By increasing this voltage, the eight channels are shifted towards lower wavelengths. The wavelength shifting is expressed in the following equation [14]

$$\delta\lambda_c = \frac{e_{LCC} \times \lambda_c}{\Delta} \times \delta(\delta n_{LCC}) \tag{1}$$

where δ (δn_{LCC}) is the birefringence variation of the liquid crystal due to an electro-optic effect. When Δ is the optical path difference of a hybrid stage, it is written as follows [14]

$$\Delta = e_{BP} \times \delta n_{BP} + e_{LCC} \times \delta n_{LCC} \tag{2}$$

δn_{LCC} is the liquid crystal birefringence. We can see from fig. 3 that the birefringence varies according to the different voltages applied. In our work, δn_{LCC} varies from 0.0081 to 0.12 by applying an AC voltage from 7.9V to 1.08V, respectively (see fig. 3).

We have taken into consideration the different insertion losses (cited in the second paragraph of this section) that were created by the twenty birefringent plates and the two linear polarizers. Hence, the designed Solc filter provides a total insertion loss without connectors of 4.63dB. It is important to note that the obtained total insertion loss is lower than the insertion losses provided by the Xtract filter (6dB) cited in reference 11 and the Teraxion tunable filter (5dB) cited in reference 12. The tunable hybrid Solc filter presents a crosstalk of 14dB.

Due to the use of several inclined polarization sensitive components (polarizers and birefringent plates), the proposed filter presents a huge polarization dependent loss (PDL) that represents an unpolarized light that propagates along the filter elements. To eliminate the excess loss, we should duplicate the 10-stage hybrid filter in two different configurations; in addition to creating separate TE and TM polarization at input through using a polarization beam splitter (PBS) (see Figure 4). At the output of the two filters, a polarization beam combiner (PBC) is used to gather the two orthogonal polarizations in order to have a filtered signal with a very low PDL. This filter has a non-rotated front polarizer, while its analyzer is inclined at a 90-degree angle. It is characterized by a front polarizer inclined by a 90-degree angle and a non-rotated analyzer. From Fig. 4 we can see that the two filters are used as TE/TM converters, which is where the two converted modes are recombined to recover the filtered signal.

Table I presents an example of a channel's wavelength shifting after it was initially centered on 1564.69nm. It also represents channel n° 16 from the 100GHz ITU grid. We can make a shift of 0.1nm by applying a voltage of 1.1V. Meanwhile, an optical phase shift of 32nm is needed in order to have a wavelength tuning step of 0.1nm. We can also displace the ITU channel, n°16 (1564.69nm), towards channel n°17 (1563.87 nm) by applying a voltage of 1.26V. In that case, the ten liquid crystal cells must simultaneously provide an optical path difference (OPD) of 935.26nm (see Table I). Slight changes in the geometrical parameters of the calcite plates and the corresponding AC applied voltages will lead to a worse performance of the proposed filter. If we change, for example, the OPD of each calcite plate from 530µm to 500µm, instead of filtering the ITU channel n° 16 (1564.69nm) the Solc filter will select channel n° 15 (1565.49nm) for the same applied voltage (1.1V). Therefore, if the OPD tolerance of the calcite plate is 30µm, we are again obliged to optimize the available applied voltage in order to select a wavelength of 1564.69nm. In any case, the same changes on these geometrical parameters do not affect the insertion loss and the crosstalk of the proposed filter.

It is important to remember that a channel's bandwidth with a Solc filter becomes narrower when increasing its stage number. We have proposed ten hybrid stages that can be used to achieve a minimum 3dB bandwidth of 0.31nm. In order to increase this bandwidth, two consecutive stages need to be eliminated; this can be done by transforming the 10-stage hybrid Solc filter to an 8-stage, a 6- stage, a 4-stage, and a 2-stage one. This achieves a maximum 3dB bandwidth of 1.4nm (see Table II). We have used the optical cancelling technique demonstrated in reference 14, for this purpose. The basic principle of this technique is to transform a half-waved hybrid stage to full-waved one. We know that a full-waved stage does not change a polarization state and, in this case, it is considered to be a transparent stage and is cancelled optically.

The OPD of a half-waved liquid crystal can be written as follows [14]

$$\Delta_{LCC}=(2k+1).\ \lambda/2 \quad (3)$$

while the OPD of a full-waved one is expressed as follows [12]

$$\Delta_{LCC}= k\ \lambda \quad (4)$$

where k is an integer.

To make this transformation, we need to subtract λ/2 from the optical thickness of the half-waved cell. Two-hybrid stages are optically cancelled if their liquid crystal cells present the following OPD:

$$\Delta_{LCC\_wave}= \Delta_{LCC\_half\text{-}wave} - (\Delta_{LCC\_half\text{-}wave} / 2) \quad (5)$$

From Table II, we can see that the minimum channel's bandwidth is obtained when simultaneously applying a voltage of 1.08V on the ten liquid